An Approach Using Low-Cost Drone Imagery with an Image Analysis Model to Evaluate Disaster Recoveries

By

Germán Camilo Buitrago

May, 2024

Director of Thesis: Daniel V. Perrucci, Ph.D.

Major Department: Construction Management

ABSTRACT

After disaster events, community leaders face the challenge of rebuilding societal infrastructure and managing the allocation of funds that can extend or reduce durations of recovery periods. Decision-makers must quickly determine how to allocate financial resources while minimizing the population distress. Conventional methods of assessing damage and evaluating relief requirements fall short of meeting the urgent recovery needs after a disaster, which could lead to negative effects on communities, such as involuntary relocation and neighborhood gentrification. This evaluates current methods and technologies and suggests a new approach using low-cost consumer drones and modern image analysis techniques to aid initial damage assessments and track recovery progress to promote dynamic appropriation. Using drone imagery allows for quick data collection and dynamic analysis, enabling multiple reviews during the disaster response and recovery phases. The study explores the potential of temporary blue tarps ("blue roofs") as a metric of recovery progress and validates the automated analysis. This research analyzes a case study of images collected during the 2020 tornado in Middle Tennessee. By providing an affordable (i.e., low-cost drones) and efficient data analysis tools (i.e., modern image analysis techniques), the goal of this research is to improve resource allocation and decision-making in post-disaster recovery efforts by government officials.

An Approach Using Low-Cost Drone Imagery with an Image Analysis Model to Evaluate Disaster Recoveries

A Thesis

Presented to the Faculty of the Department of Construction Management

East Carolina University

In Partial Fulfillment of the Requirements for the Degree

Master Science in Construction Management

By

Germán Camilo Buitrago Cagua
May, 2024

Director of Thesis: Dr. Daniel V. Perrucci,
Thesis Committee Members:
Kathleen Short, PhD
George Wang, PhD
Yilei Huang, PhD

ACKNOWLEDGMENTS

I would like to express my gratitude to my advisor Dr Daniel Perrucci, for his invaluable guidance and support. His expertise, patience, and commitment have been instrumental in shaping my academic growth. I´m also deeply thankful to my family, their love and belief in me have been the foundation of my determination to overcome challenges.

TABLE OF CONTENTS

ACKNOWLEDGMENTS iii

LIST OF TABLES vi

LIST OF FIGURES vii

CHAPTER 1: INTRODUCTION 1

Problem Statement 1

Goal and Objectives 2

CHAPTER 2: LITERATURE REVIEW 3

Disaster Funding Appropriation 3

Post-Disaster Damage Evaluation 3

Impacts of Social Vulnerability 4

Gentrification and Cultural Loss 5

Historical Usage of UAV Imagery 5

Image analysis on drone imagery 6

Low-Cost Consumer Based Drones 7

Operation Blue Roof 8

Image Analysis (MIPAR) for Tracking the Blue Roof Implementations 9

CHAPTER 3: METHODOLOGY 10

Case Study 10

Location 1 – East Nashville, TN 11

Location 2 – Mt. Juliet, TN 12

Tracking “Blue Roofs” with Iterative Image Analysis 13

CHAPTER 4: RESULTS 15

Automated Model Validation 16

Raw Area vs. Fixed Area of Blue Roofs 16

Percent Error Validation 21

R-Squared Validation 23

CHAPTER 5: DISCUSSION 29

September 29 East Nashville Location 1 29

March 29 Mt Juliet Location 1 31

June 12 Mt Juliet Location 2 33

CHAPTER 6: CONCLUSIONS 36

REFERENCES 39

APPENDIX 44

LIST OF TABLES

Table 1: Tornado Path with Severity and Impacts 11

Table 2: Error Percentage Calculations 22

Table 3: R-Squared Values for Each Location 25

Table 4 Pixel Area Data Before and After Correction Process 44

LIST OF FIGURES

Figure 1: East Nashville Tornado Damage 12

Figure 2: Mt. Juliet Tornado Damages 13

Figure 3: Drone Image Analysis Implementation to Identify Tarped Roofs 14

Figure 4: East Nashville Preliminary Trends 15

Figure 5: Mt Juliet Preliminary Trends 16

Figure 6: Fixed data & Raw data East Nashville Location 1 17

Figure 7: Raw Data and Corrected Data East Nashville Location 2 18

Figure 8: Raw Data and Corrected Data Mt Juliet Location 1 19

Figure 9: Raw Data and Corrected Data Mt Juliet Location 2 20

Figure 10: Linear Regression East Nashville Location 1 25

Figure 11: Linear Regression East Nashville Location 2 26

Figure 12: Linear Regression Mt Juliet Location 1 27

Figure 13: Linear Regression Mt Juliet Location 2 28

Figure 14: East Nashville, location 1, 4th September. 30

Figure 15: Mt Juliet, Location 1, March 29, 2020. 32

Figure 16: Mt Juliet, Location 2, 12th June 2020. 33

CHAPTER 1: INTRODUCTION

Problem Statement

Natural hazards challenges include infrastructure reconstruction and the allocation of governmental resources. A hazard-impacted community can take several years to achieve a full recovery and often relies on governmental relief. If governmental relief is insufficient, non-governmental organizations (NGOs) are recognized as an alternative [1][2].

The hazard-impacted population is vulnerable throughout the recovery period, and attributes that contribute to vulnerability, such as age, gender, race, unemployment rate, education level, and socio-economic status can vary impact capacity and alter recovery periods. In the case of housing displacement after a natural hazard, a lack of required resources for recovery can lead to gentrification and increases in the community's pre-hazard cost of living. The debate over the best methods to evaluate social vulnerability is ongoing. However, multicriteria decision analysis combined with geographical information systems (GIS) can quantify and map social vulnerability scenarios [3][4][5].

Damage evaluation utilizing traditional survey methods is challenging due to the resource and time consumption. Likewise, satellite imagery offers an efficient means to interpret damage in buildings but introduces high internal variability due to low granularity [6][7]. Decision-making for post-disaster recovery occurs under pressure to rebuild, making traditional mapping and valuation challenging due to limited resources and a restrained number of volunteers. The utilization of drone imagery is a promising technology for rapid data collection and dynamic analysis (e.g., multiple reviews) during hazard response and recovery. The use of drones offers

cost-effective and efficient evaluation of hazard impacts, enables the identification of areas requiring immediate or increased attention, and provides verifiable data to support the development of recovery plans [8][9][10].

Goal and Objectives

This study begins by reviewing existing methods for disaster evaluation and tracking post-disaster recoveries. The goal of the present case study is to provide a proof of concept for a novel approach utilizing drone imagery and visual recovery cues to evaluate disaster recovery. More specifically, this study aims to create an evaluation methodology leveraging the benefits of low-cost consumer drones empowered by modern AI image analysis to promote dynamic appropriation based on a "blue roof" metric. The benefits and limitations in using low-cost consumer-grade Unmanned Aerial Vehicle (UAVs) for disaster response and recovery is explored. Results indicate that a viable recovery metric is possible through the analysis of consumer-grade UAV imagery. The utilization of consumer drones offers a cost-effectiveness and efficiency in data collection, which in turn mitigates accessibility concerns during the collection period and cost limitations associated with sophisticated professional drones.

CHAPTER 2: LITERATURE REVIEW

Disaster Funding Appropriation

After a natural disaster (e.g., tornados, earthquakes, floods, and forest fires), the impacted communities can require several years to fully recover [11][12]. These disasters can cause important impacts including personal and financial losses that can lead to bankruptcy [13][14]. When a disaster occurs in the United States, the federal government supports the impacted population with relief in the form of funding. In 2020, the United States experienced a record of 22 weather or climate disasters that resulted in at least $1 billion in damages [15]. In some cases, federal funds are limited, and non-government organizations (NGOs) are common alternate resources individuals depend on [2][7].

The primary ways to reduce the direct economic cost from a natural hazard event include, but are not limited to, implementing mitigation methods to reduce the severity and cost sharing (e.g., government; charitable aid; insurance) to relieve the financial impact on affected communities. In the United States, disaster response funds funnel through the Federal Emergency Management Agency (FEMA) and specialized catastrophic insurance programs. In recent years, these programs have been criticized for lacking financial sustainability [1]. The incorporation of consumer-grade technologies addresses accessibility and cost associated with high-end solutions.

Post-Disaster Damage Evaluation

FEMA describes their response after a disaster in three phases: the emergency response phase, the relief phase, and the recovery phase. FEMA uses different scales to grade the damage.

At two extremes, gathering recovery data from elicited surveys is resource-intensive in terms of time and human effort. In contrast, satellite imagery enables a fast-paced interpretation of damage in some structures that can introduce internal variability from events like flooding [16][17]. The limited resources, difficulty in mobilizing in the area, and dependence on a limited volunteer base in disaster scenarios demand innovative methods for the evaluation of disaster phases. The utilization of UAVs is one example of the implementation of new technologies on the collection of data based in aerial imagery for post-disaster damage evaluation. Data analysis methods are also improving, specifically with the implementation of artificial intelligence that enables a faster evaluation of imagery [18][19][20].

Impacts of Social Vulnerability

Vulnerability contains several aspects, including unemployment, education and modifies sociodemographic behavior, restricting the capacity of the society to handle hazard events [3]. The evaluation of social vulnerability in some cases, includes variables, such us, age, gender, race, ethnicity, social class, unemployment rate, immigrant status and quality of the built environment. Debates have emerged regarding the possibility of establishing a set of parameters that can define social vulnerability regardless of the level of hazard exposure. The process of evaluating social vulnerability entails several steps: (1) establishing a hierarchical structure for the social vulnerability model, (2) standardizing the criteria, (3) assigning weights to the criteria, and (4) implementing decision rules and mapping social vulnerability scenarios. Multicriteria decision analysis (MCDA) is a configuration of methods for scale decision alternatives based on multiple conflicting criteria and selecting the best alternative. This method is combined with GIS (geographic information system) to evaluate what and who is at risk. By analyzing vulnerability

from a social perspective, disaster management can develop successful risk planning and management strategies to decrease the impact of the affected population [4][21].

Gentrification and Cultural Loss

Population affected trends to be forced to relocate into a new-build urban society. Gentrification describes the process of renovating and revitalizing working-class and neglected housing, leading to the subsequent translation of an area into a middle-class community [22][23]. This growth affects the residents and the community, increasing the cost-of-living. Governments have devised methodologies for measuring and mapping gentrification risk. It is important to note that each model considers distinct variables in its assessment. For instance, The Displacement Risk Index (DRI), was created by the Seattle Office of Planning & Community Development; Los Angeles Index of Displacement Pressure (LAIDP) was created by the Los Angeles Innovation Team to reduce displacement, and another methodology is the Portland Gentrification and Displacement Risk (PGDI). On the other hand, the city of Philadelphia develops their measure in a study of gentrification effect on residential mobility rates [24].

Historical Usage of UAV Imagery

Natural disasters such as hurricanes, floods, and earthquakes have profound economic, social, and political impacts that are driving updates to measurement and methodologies [18]. The main limitations to current measurement and mitigation methodologies include, but are not limited to, reduced accessibility options. For instance, consider the tsunami and earthquake that occurred in Japan during 2011. In this scenario highways and railways were blockaded by the debris or destroyed, limiting transportation routes [19]. The associated costs of post-event reconnaissance in the impacted regions can increase due to similar infrastructure damages [25].

UAVs are aircrafts that operate without a human pilot on board. These aircrafts are remotely controlled and can be used for different purposes, including data collection, monitoring, surveillance, and other applications in different industries [26]. The use of this technology offers advantages in different contexts. In the humanitarian realm, the use of UAVs has extended from global battlefields to zones of humanitarian emergencies. Nevertheless, the adoption of UAVs remains a subject of disagreement among certain authors. The use of military drones being labeled as "humanitarian weapons" requires careful examination of the ethical and political effects within both a global and regional context [27]. However, this technology has shown its cost-effectiveness in a range of post-disaster and environmental applications.

The incorporation of low-cost consumer UAV quadcopter drones in UAV imagery analysis for disaster recoveries suggests a cost-effective solution, providing flexibility and affordability in data collection and analysis. This technology promotes the achievement and analysis of UAV-based aerial imagery. Optimization on workflow involving the flight planning, data acquisition, post-processing data delivery and sharing of orthomosaic maps that can be shared with different public and private stakeholders can help to optimize the process of post disaster analysis [28][28][10].

Image analysis on drone imagery

Drone imagery analysis innovation in large-scale traffic monitoring can promote the implementation for disaster recoveries, with the integration of low-cost consumer drones. The results from this study can provide evidence that advanced deep learning techniques can assist in evaluating human activity when paired with drone imagery technology. These applications of

image analysis on traffic monitoring reveal a six times higher detection speed, enhanced adaptability on difficult ambient conditions and stronger detection robustness [29].

Modern use of image analysis is shown in autonomous vehicles, computer vision from objects, face detection from UAVs, and enhanced surveillance capacities. The challenges include maintaining accuracy, variations in scale, overlapping objects/views, and lighting conditions in different scenarios [30]. Optimization approaches, artificial intelligence, and hardware accelerators can assist in achieving real time [31].

Low-Cost Consumer Based Drones

Low-cost consumer drones offer advantages for disaster recovery and evaluation efforts. These types of drones are affordable and significantly cheaper compared to professional-grade drones [32]. A price comparation between a professional drone (e.g., DJI MATRICE 350 RTK, $18,000.00) and the drone utilized on this analysis (i.e., DJI MAVIC MINI 2, $300.00) raise a total percentage savings in 98.3% [33][34]. These initial drone purchase cost savings is crucial, especially for governments, organizations, and population with limited budgets that are already being stressed during an extreme scenario (e.g., natural hazard). Any cost savings can be re-allocated to assist with other recovery and relief activities. The wholesale availability of consumer drones also ensures that they are accessible for emergency deployment in disaster affected areas, facilitating rapid response and data collection [35].

Low-cost consumer drones also present some limitations, the lack of GPS control, which can affect the precision of data collection. Additionally, consumer drones may face problems with stabilization, developing blurred images and reduced image quality. These challenges associated

with low-cost drone image collection can potentially affect the effectiveness of recovery evaluation but the minimized financial investment warrant further investigation. Furthermore, advancements in technology, such as the integration of modern image analysis and artificial intelligence promise solutions to mitigate these challenges associated with low-cost consumer drones and enhance their capabilities on disaster assessments and recovery efforts [36][37].

The range of modern UAVs (consumer and commercial) available on the market offer diverse options that can vary significantly in price and resolution. For this research, a DJI Mavic Mini 2 is utilized for data collection with a 12-megapixel (MP) camera resolution. In a maximum image size of 4000x3000 pixels, a single pixel represents the smallest units of visual information, and similar pixels can be grouped together to represent total pixel area of the attributes being analyzed. This granularity provided by 12,000,000 pixels enables detailed analyses and facilitates the extraction of valuable insights from aerial imagery [38] [39].

Operation Blue Roof

Operation Blue Roof, a program managed by the U.S. Army Corps of Engineers for FEMA, is instrumental in the aftermath of natural disasters. Operation Blue Roof focuses on providing homeowners in disaster areas with fiber-reinforced plastic sheeting to cover damaged roofs temporarily until repairs can be carried out.

This initiative works a dual purpose by safeguarding property and possessions against environmental exposure and reducing temporary housing costs for affected residents. The significant aspect of Operation Blue Roof is its ability to allow homeowners to remain in their

residences during the recovery phase, fostering a detect of normality and connection amidst the disruption caused by the natural disaster [40].

Image Analysis (MIPAR) for Tracking the Blue Roof Implementations

A software known as MIPAR is utilized for image analysis in this study to quantify the pixel area of Blue Roofs for the data analysis. This software offers advanced automation capabilities for detecting defined attributes in images [41] The model utilized in this study is trained using a dataset configured by six of the eight image dataset. In this model, the images are analyzed in nine distinct layers to isolate objects such as houses, blue roofs, vegetation, cars, yards, the sky, roads, and debris piles. The primary objective set during the model's training process is to accurately measure the area of blue roofs in the selected image on a specified data.

CHAPTER 3: METHODOLOGY

Case Study

A case study is a deep analysis of an event or phenomena that is conducted to get an understanding of unique contexts/implications (e.g., hurricanes and tornadoes)[10]. This study utilizes the 2020 Tennessee Tornado as a case study, to categorize the severity of tornadoes using the Enhanced Fujita scale (EF), oscillating from EF-0 (contemplate a weak class) to EF-5 (categorized as violent tornado). The EF scale incorporates 28 different variables, factors such as the type of building, existing structures, and tree coverage should be taken into consideration. This scale offers a more complete perception of how tornadoes affected the impacted areas [42]. This case study helps us to understand the feasible use of drone imagery technology to evaluate the recovery process on the affected area.

On March 2-3, 2020, a series of devasting tornadoes touched down across middle Tennessee [43]. The supercell responsible for this destructive natural hazard was initially formed near the Mississippi River, and spawned a total of 15 tornadoes, between EF-0 TO EF-4 by the Enhanced Fujita rating, including a high-end EF3 tornado that hit Nashville [44]. This event resulted in 25 fatalities, with an additional 309 people injured [45]. According to the National Centers for Environmental Information, the tornado damage reached around $95.0 billion [15]. The path of the tornadoes presented on the event is organized in Table 1.

Table 1: Tornado Path with Severity and Impacts

Severity	County	State	SVI	Deaths	Property Damage ($)	Crop Damage ($)	Source
EF1	Gibson	TN	0.783	20.87	57,072,784.10	13,584,660.53	[46] [47] [48]
EF2	Carroll	TN	0.549	15.87	24,388,916.97	1,988,160.53	[49]
EF2	Benton	TN	0.442	9.88	20,937,195.24	1,536,635.58	[50]
EF1	Humpherys	TN	0.307	42.87	211,725,673.40	2,307,170.33	[51]
EF3	Davidson	TN	0.692	67.74	2,889,424,919.00	1,825,619.35	[52]
EF3	Wilson	TN	0.174	7.74	474,540,746.7	2,311,919.35	[53]
EF1	Smith	TN	0.386	3.12	15,816,540.58	1,851,453.02	[54]
EF4	Putnam	TN	0.637	31.12	149,978,659.00	2,095,653.02	[55]
EF2	Cumberland	TN	0.433	7.62	41,321,025.03	1,888,480.39	[56]
EF0	Morgan	TN	0.688	9.12	5,390,225.63	1,455282.06	[57]

Location 1 – East Nashville, TN

East Nashville, TN is an area situated in the eastern part of downtown Nashville TN that incorporates residential and mixed-use areas with a population of approximately 77,688. By covering an area of 20,533 square feet, East Nashville has a population density of 3,784 people per square mile. The average income on a median household is $70,014. In terms of racial demographics, the community is composed by, 49.1% white residents, 25.7% black residents, 8.4% Hispanic or Latino residents, 5.4% Native Hawaiian and Other Pacific Islander residents,

4.1% Asian residents, and 4.1% two or more races, with an additional 2.8% belonging to some other racial background [58]. On March 2, 2020, more than 30 business were destroyed with nearly 40 structures collapsing [59].

Figure 1: East Nashville Tornado Damage

Figure 1 illustrates East Nashville (EF-3) post-natural hazard affected zone, displaying two different angles of the damaged infrastructure and the ongoing recovery effort process of the affected community.

Location 2 – Mt. Juliet, TN

Mt. Juliet, TN also known as Mount Juliet, is a city located in western Wilson County, TN. Mt. Juliet claims to be the "fastest-growing city in Tennessee" and has a total area of 16.6 square miles with a population of around 40,000 residents. The estimated median household income in 2021 was $97,112. In relation to racial demographics, Mt. Juliet is composed by 78% White residents, 6.6% Hispanic residents, 6% Black residents, 4% Asian residents and 2.3% other racial backgrounds [60]. This town faced challenges during the recovery process due to the severity of the tornado and the limiting factor of the coronavirus pandemic that require safety precautions

and isolations. An example of the impact to these limitations was the pending year period for Mt. Juliet public schools to hire a contractor for reconstruction of the damaged infrastructure [59].

Figure 2 provides the aftermath of the tornado in Mt Juliet (EF-3) posing a comparative perspective on the extent damage and recovery process.

Figure 2: Mt. Juliet Tornado Damages

Tracking "Blue Roofs" with Iterative Image Analysis

A series of collected iterative drone images in response to the 2020 tornado in Tennessee comprises the data for this study. These images were collected on eight individual dates including March 11, March 15, March 21, March 29, April 4, April 11, June 12, and September 4, to monitor and track disaster relief and response activities that can assist in achieving recovery. In this image collection, four drone take-off locations were utilized, and significant attempts are made to maintain consistent image attributes (e.g., height, angle, weather, location, frame) with limitations due to the utilization of low-cost consumer UAV quadcopter drones. An image analysis software is utilized to automate the tracking of "blue roofs", an attribute of disaster response that can indicate and provide a metric for recovery.

The process of quantifying roof damage in images is conducted on a model with a training set of six representative images and a set of twelve testing images. Within these images, nine distinct categories or layers were defined, each designated by unique colors. These categories encompassed elements such as houses, blue roofs, grass, cars, yards, sky, roads, debris, and trees. The primary objective of this model was to estimate the change in roofing damage over time. On implementation, this model efficiently identifies blue roofs, marked in red and quantifies these areas in pixel units. Corrective actions are possible if classification is inaccurate. The output of the automated identification and potential false positives are shown in Figure 3.

Figure 3: Drone Image Analysis Implementation to Identify Tarped Roofs

The image analysis software is made by the 4k image resolution and utilizes a pixel-level analysis of each image in the iterative collection to identify tarped roofing. The analysis quantifies pixel density within an area, with each pixel representing a single point within that image. By employing this pixel analysis with iterative image collection, the pixel area, and change over time can be quantified and analyzed as a metric for disaster recovery.

CHAPTER 4: RESULTS

The analysis produces results for two locations in East Nashville, TN and two locations in Mt. Juliet, TN. A total of 16 images were obtained and analyzed to track the change in "blue roof" pixel area on eight specific dates over a 7-month period. Figure 4 and Figure 5 shows the trends in "blue roof" activity from the model.

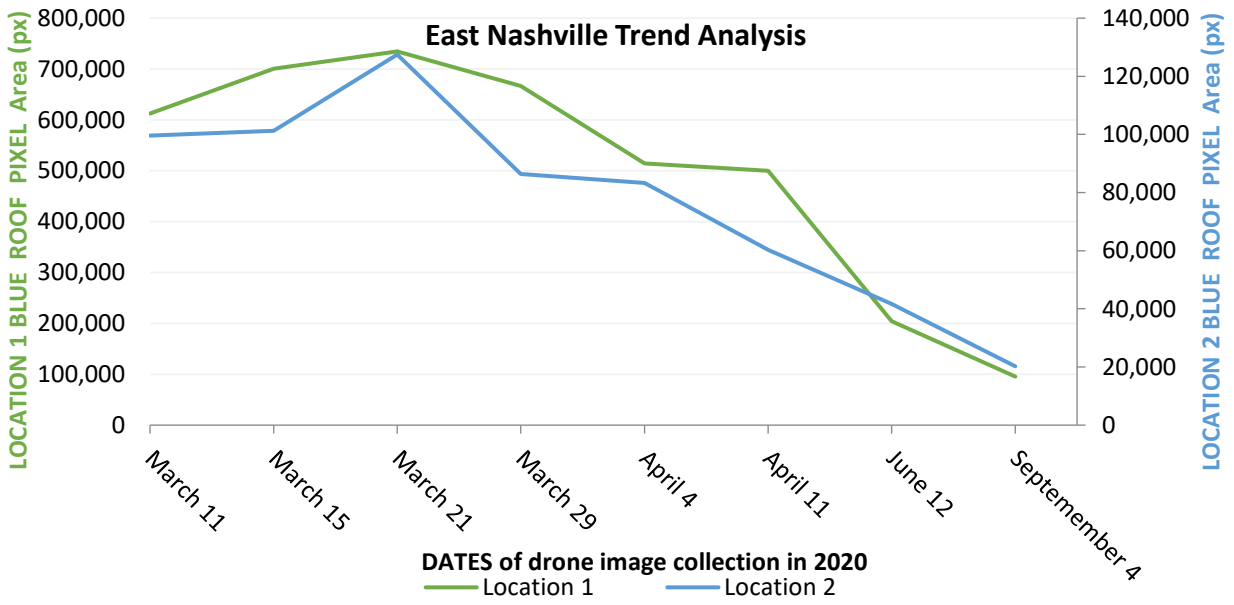

Figure 4: East Nashville Preliminary Trends

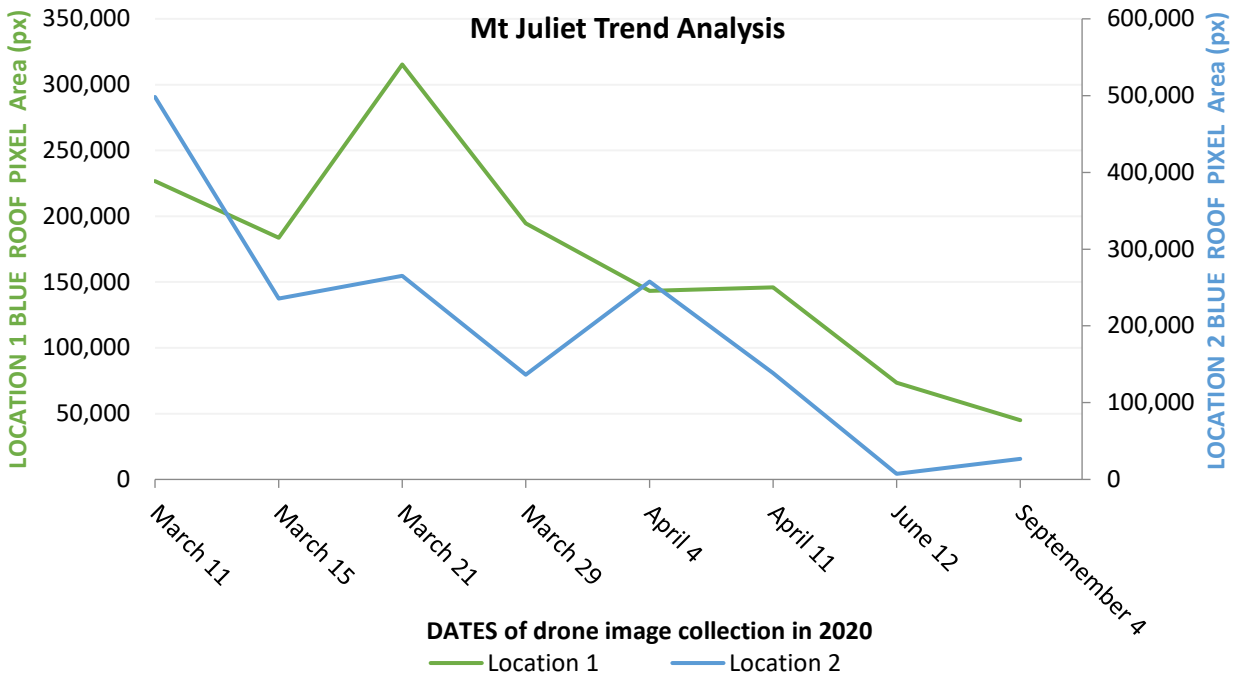

Figure 5: Mt Juliet Preliminary Trends

In Figure 4 and Figure 5, the y-axis of the graph shows the number of pixels that form a blue roof in each photo taken on the dates expressed on the x-axis. The graph shows a reducing trend in the number of "blue roofs" towards the end of those seven months, highlighting that the quantified results from automated analyses of post-disaster UAV imagery can act as an effective metric for progress towards recovery. These results show a trend in the reduction of "blue roofs" up to that seven-month period. The same approach is applied to Mt. Juliet, TN for the image set.

Automated Model Validation

Raw Area vs. Fixed Area of Blue Roofs

The validation of this proof of concept begins with an initial view of the quantified raw "blue roof" area that includes false positive "blue roof" identifications and a corrected quantification with false positive "blue roof" identifications removed. The analysis has successfully produced results for four specific locations in East Nashville, TN and Mt. Juliet, TN, respectively.

Figure 6 presents the data that provides a visual representation of the "Blue Roof Pixel Area" on the y-axis with area quantification, including false positives in blue and a corrected area with false positives removed in red.

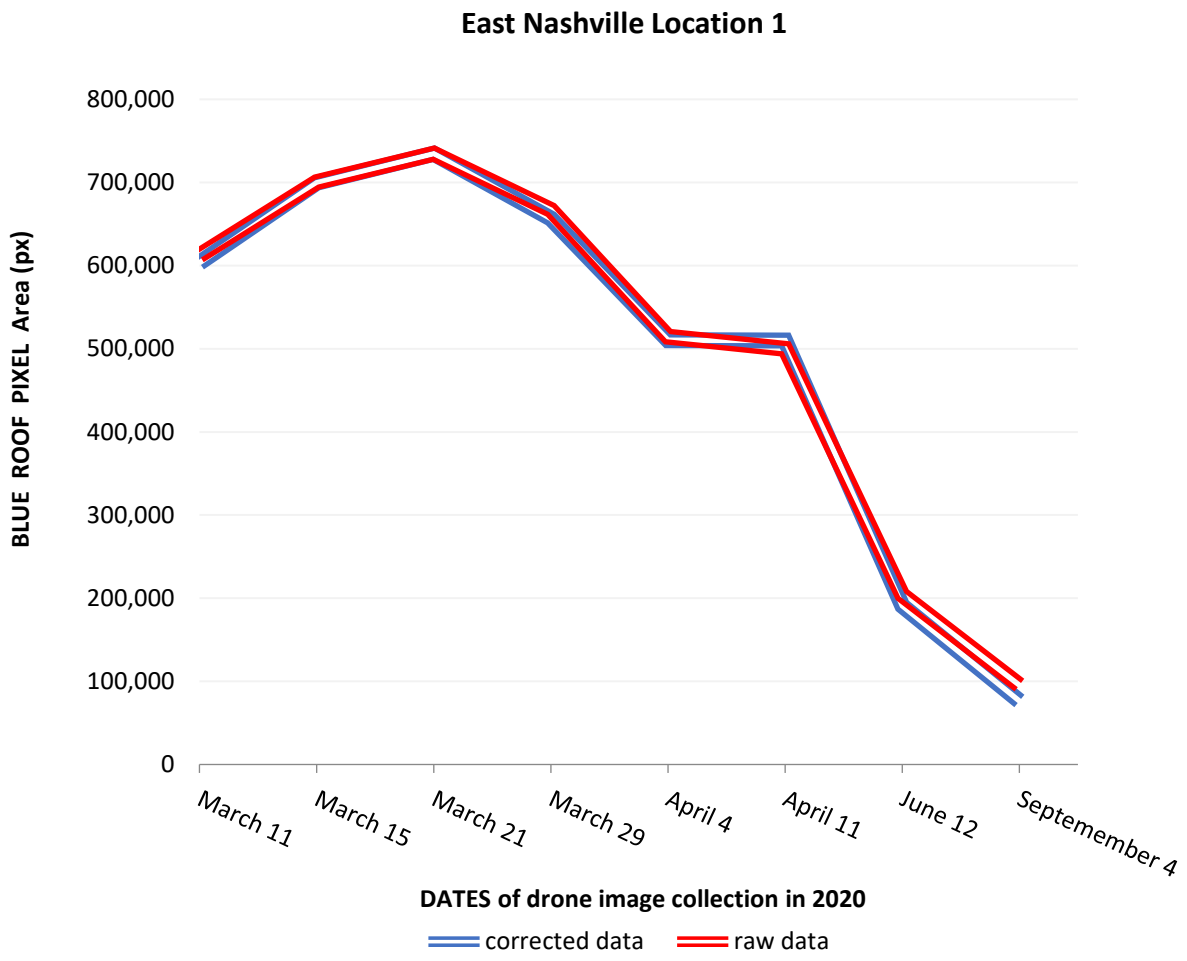

Figure 6: Fixed data & Raw data East Nashville Location 1

This initial view of the raw and corrected "blue roof" areas reveals minimal deviation, with a false positive impact only growing in the last two months.

The plot Figure 6: Fixed data & Raw data East Nashville Location 1 illustrates the graphical representation of both data types over the seven-month period. The results for this location exhibit similarities, suggesting minimal impact from false positives.

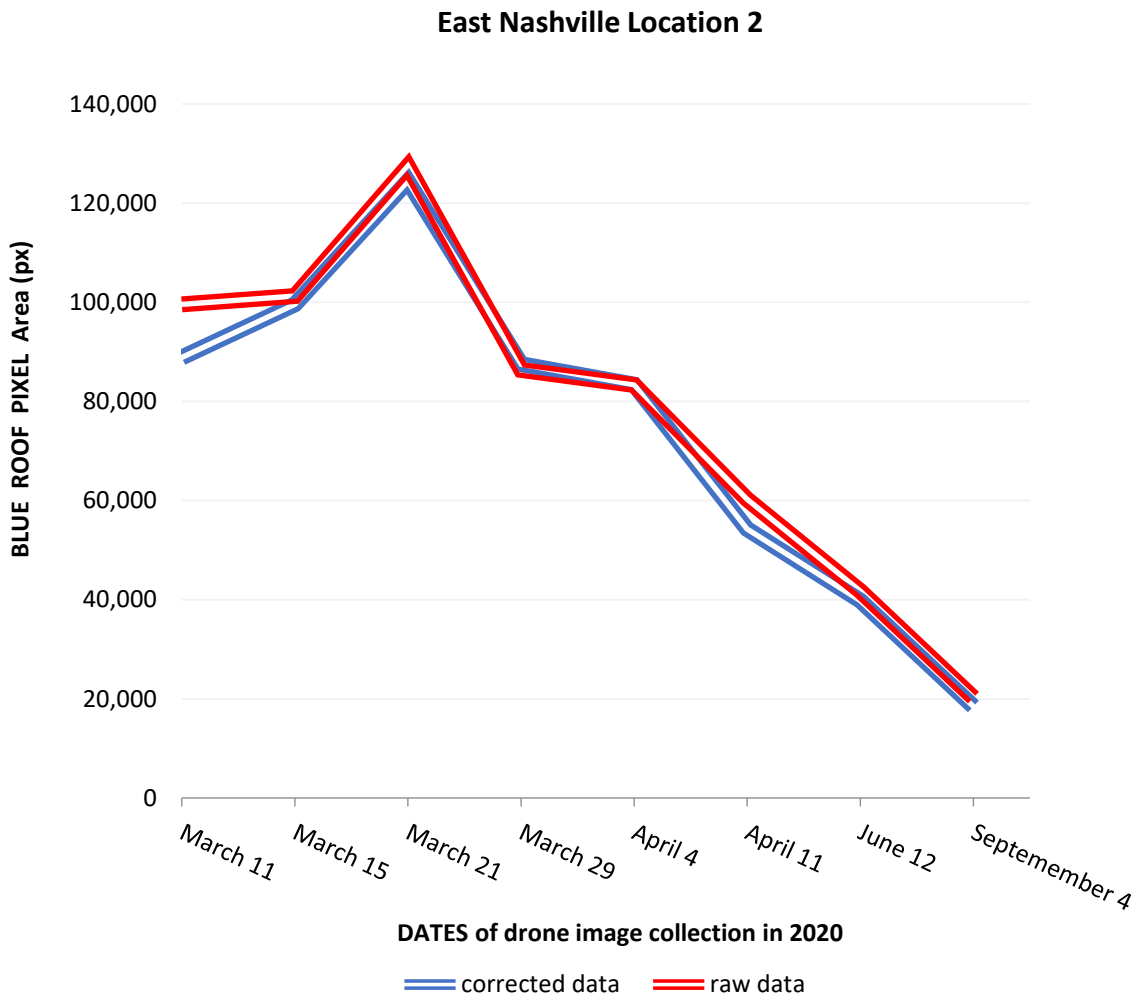

Figure 7: Raw Data and Corrected Data East Nashville Location 2

On analyzing Figure 7: Raw Data and Corrected Data East Nashville Location 2 which illustrates the recovery process after the natural hazard, distinct patterns emerge. A notably alteration in the values on the first date of the evaluation process, this difference in values will be quantified and

elaborated in the subsequent subsection of the results section, where various methodologies are employed to assess this differentiation comprehensively. Although the initial differences, the curves illustrating fixed (blue) and raw (red) data exhibit alike behavior across the majority of evaluated dates, suggesting consistent trends in the recovery dynamics over time. Moreover, the reduction in the number of pixels associated with blue roofs highlights a recovery trend that, predominantly for this location, increases the false positives influence as the "blue roof" recovery finalizes.

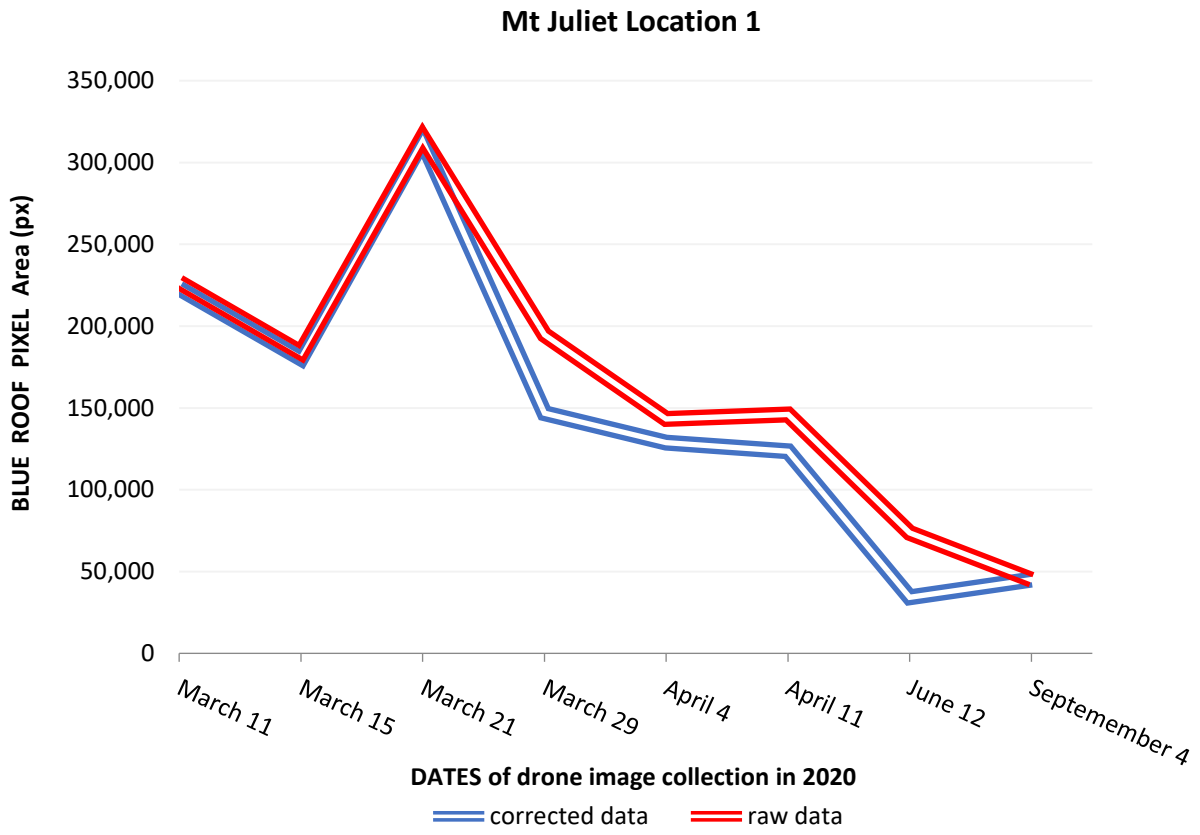

Figure 8: Raw Data and Corrected Data Mt Juliet Location 1

In Figure 8, the recovery trend (i.e., reduction in blue roofs) shows variability after the third collection date on March 21. The largest of the variability between raw and correct blue roof

identification, on June 12 and September 4, there is an increase in the corrected area and a decrease in the raw area. The raw data initially detected lower levels of blue roof pixels, expected with the decreasing trends of blue roof utilization associated with on-going recoveries, that increases the influence of false positives. The affect of false positives later in recoveries is expand investigated in the discussion.

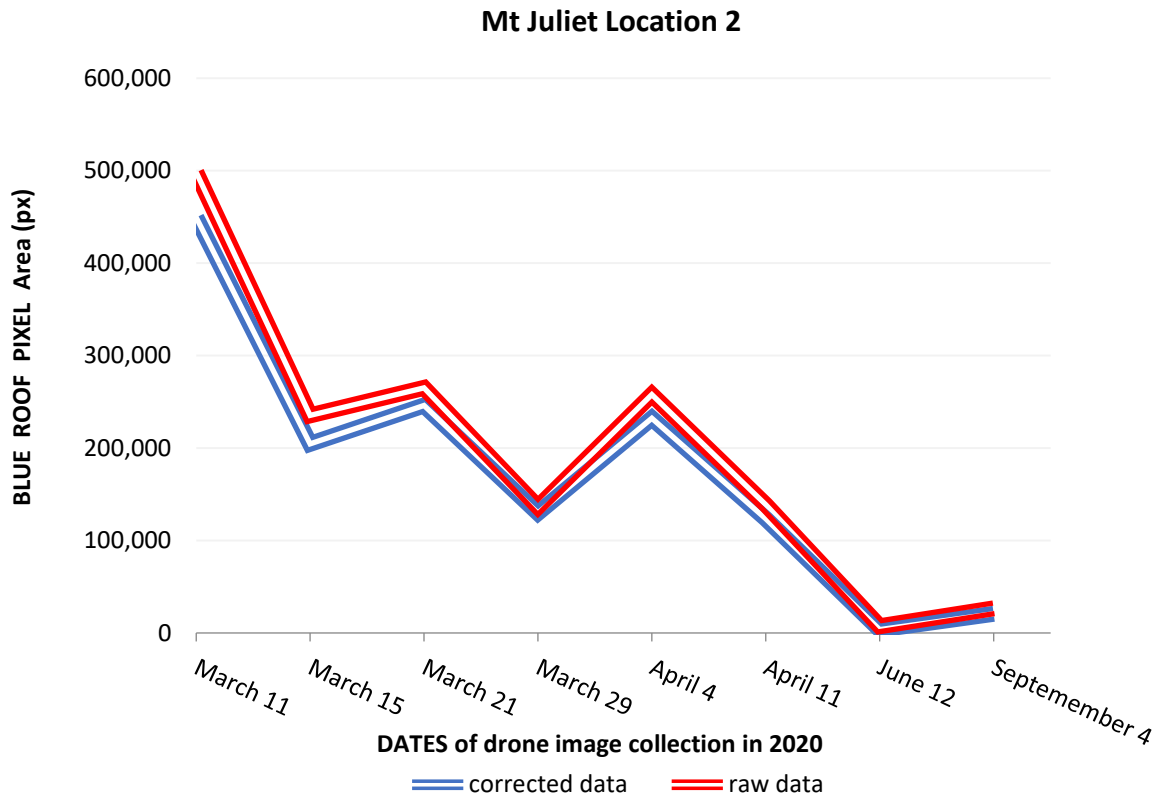

Figure 9: Raw Data and Corrected Data Mt Juliet Location 2

Figure 9: Raw Data and Corrected Data Mt Juliet Location 2, suggests a close orientation between the raw data and corrected data. The aligned variations in blue roof trends may be attributed to distinct phases within the recovery process. For instance, the fluctuations may correspond to phases where houses are assigned for demolition (i.e., blue roof reduction) or where reconstruction efforts commence (i.e., blue roof increase).

From East Nashville to Mt Juliet, each location presents distinctive challenges. The observed trends across different locations impacted by the same hazard event underscores the applicability of the methodology in explaining the multifaceted dynamics of the recovery process across different settings. The close alinement observed between fixed and raw data underscores the robustness of the evaluation process, while subtle variations reveal a need of other analysis. The comprehensive examination of correct and raw data offers an opportunity to validate the effectiveness of the data processing methodology.

Percent Error Validation

Percent error analysis is a practice used to examine the accuracy of data processing methods and identify discrepancies that require improvement. This method allows for examination of the differences between the original and adjusted datasets, enabling insights into the effectiveness of the processing techniques deployed. By identifying areas of divergence, chances for enhancing the accuracy and consistency of the assessment process emerge. [61]

The calculation of the percent error is a difference of raw and corrected data. By comparing the raw blue roof pixel area data with the validated blue roof pixel area data, the percentage error quantifies the discrepancy between the two datasets. This method poses a clear indication of the effectiveness of the data processing algorithm, highlighting areas where discrepancies arise and allowing for targeted improvements. The formula used for this calculation is shown below.

$$\frac{x - y}{y} * 100$$

where X represents the raw data and Y the corrected data, enables a standardized evaluation of the error across different datasets and locations. An error percentage between the raw and

corrected quantification of less than 10% is considered acceptable for this proof-of-concept study. These results are organized in Table 2.

Table 2: Error Percentage Calculations

Error Percentage				
Dates in 2020	East Nashville Location 1	East Nashville Location 2	Mt Juliet Location 1	Mt Juliet Location 2
March-11	1.50	12.08	1.65	10.86
March-15	0.11	1.67	2.01	15.05
March-21	0.01	2.45	0.72	7.73
March-29	1.54	-1.32	5.12	5.12
April-4	0.84	-0.12	11.12	10.99
April-11	-1.98	11.04	12.35	12.35
June-12	6.87	4.89	53.47	18.27
September-4	24.98	9.59	0.00	28.98

The Table 2: Error Percentage presents a complete overview of the error percentages across the locations and dates in 2020. Each row corresponds to a specific date, while each column represents a different location within these areas. The negative and positive values in the table indicate the deviation of the validation blue roof pixel area from the raw blue roof pixel area, expressed as a percentage. For instance, negative percentages indicate an underestimation of the blue roof pixel area by the software, while positive percentages suggest an overestimation.

The results of this analysis show an increase in the percentage error during the final dates of the evaluation process. This trend is notable in areas where the number of pixels representing blue roofs decreases towards the end of the assessment period. The observed increase in percentage error during the later stages of evaluation can be attributed to several factors, one of which is the diminishing blue roof area. In cases where the fixed area is reduced, the effect of false positives becomes more pronounced, thereby influencing the percent error (i.e., less raw area, more impact of miscalculated area). This study gains a deeper insight of these trends and their original precision through employing linear regression.

R-Squared Validation

Linear regression is a statistical framework to model the association between these datasets, providing a metric to evaluate the influence of the false positives. The linear regression model estimates the line of best-fit through the data points [62]. The Pearson correlation coefficient (r) is a measure of the linear relationship between two variables[63], with the essential purpose of the discerning correlations within the data through Equation *1*.

Equation 1: Linear Regression $$Y = m * X + b$$

In Eq 1, the variable m represents the slope of the line, while X is the independent variable, b is the interception in the Y axis of the line. Once the regression line is fit, the R-squared is calculated as the proportion of the total sum of squares (TSS) that is explained by the regression model. The TSS represents the total variability in the dependent variable, and it is calculated as the sum of the squared differences between each observed dependent variable value and the mean of the dependent variable.

Equation 2: Total sum of squares (TSS) $TSS = \sum_{i=1}^{n}(yi - \bar{y})^2$

In Eq 2, n represents the number of data points, the variable yi is the observe value of the dependent variable at data point i and $\bar{y}$ is the mean of all observed values of the dependent variable. The residual sum of squares (RSS) is also computed, which represents the unexplained variability in the dependent variable for the regression model.

Equation 3: $Residual\ sum\ of\ squares\ (RSS)$ $(RSS) = \sum_{i}^{n}(yi - \widehat{yi})^2$

In Eq 3, n represent the number of data points, yi is the value of the dependent variable at data point i, $\hat{y}i$ is the predicted value of the dependent variable at the data point i. Finally, R-squared is calculated

Equation 4: $R - squared\ coefficient\ (R^2)$ $R^2 = 1 - \frac{RSS}{SST}$

The coefficient of determination R^2 is calculated as is shown in Eq 4, RSS is the sum of squares due to error while SST is the total sum of squares. A higher R-squared value indicates a better fit of the regression line to the data points (i.e., a larger proportion of the variance in the dependent variable is explained by the independent variable). Consequently, R-squared serves as a measure of the strength on the relationship between the variables and the regression model. It ranges from 0 to 1, where 1 indicates a perfect fit, implying that all variability in the dependent variable is accounted for by the independent variable(s) [58][64]. This study sets the maximum r-squared deviation at .05 to meet the requirements for validation. Table 3: R-Squared Values for represented the different values of R-squared.

Table 3: R-Squared Values for Each Location

Location	R-squared
East Nashville Location 1	0.999
East Nashville Location 2	0.988
Mt Juliet Location 1	0.983
Mt Juliet Location 2	0.998

This table offers a overview of the R-squared values and preliminary correction of the automated image analysis methodology. The high R-values in each location signify the limited influence of false positives.

To further analyze these R-value calculations, a graphical representation of the R-squared values illustrates the relationship between raw and corrected data for each collection period. East Nashville location 1 is visualized in Figure 10.

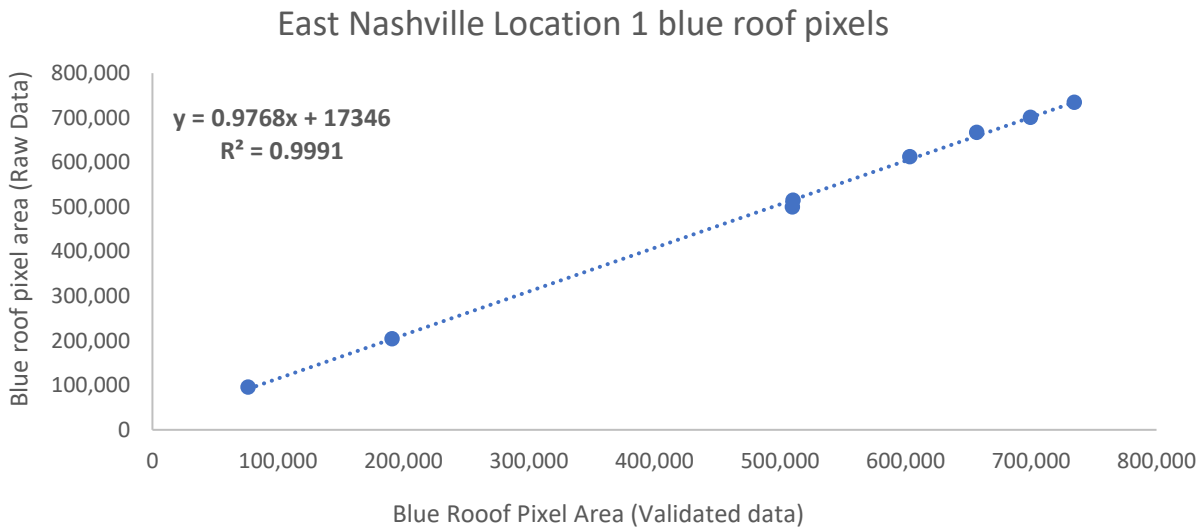

Figure 10: Linear Regression East Nashville Location 1

In Figure 10: Linear Regression East Nashville Location 1 there is a strong correlation between

the raw data and corrected data. The R-squared value is 0.999, indicating that 99.9% of the variability observed in the raw data is also observed in the fixed data.

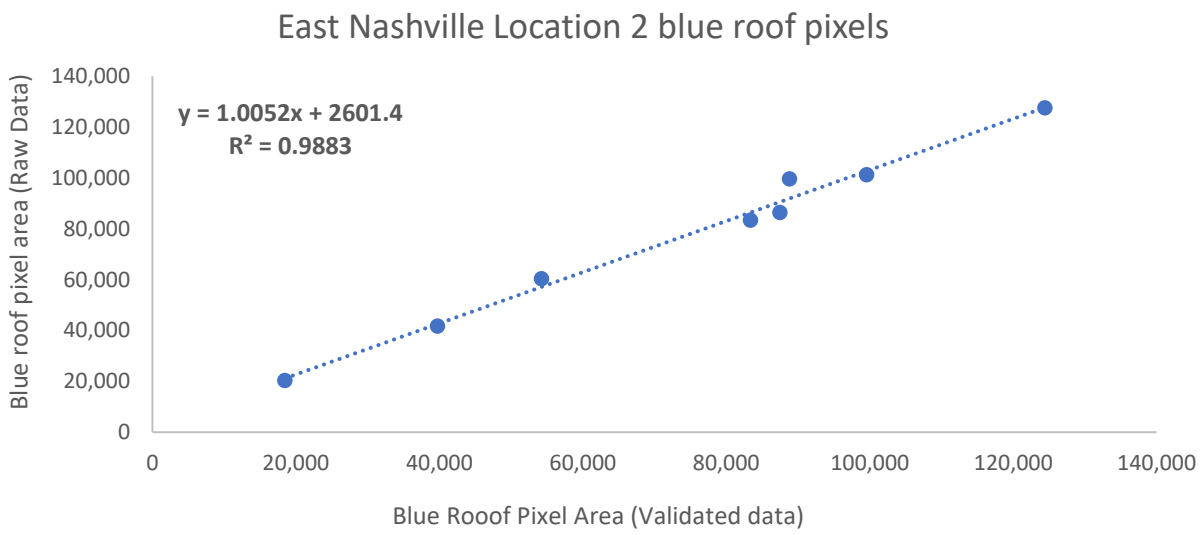

Figure 11: Linear Regression East Nashville Location 2

The linear regression analysis for East Nashville's second location is represented in Figure 11. The R-squared value is 0.988, indicating that approximately 98.8% of the variability observed in the raw data is also observed in the fixed data. These results show a desirable R-squared values but do show minor deviations between raw and corrected data.

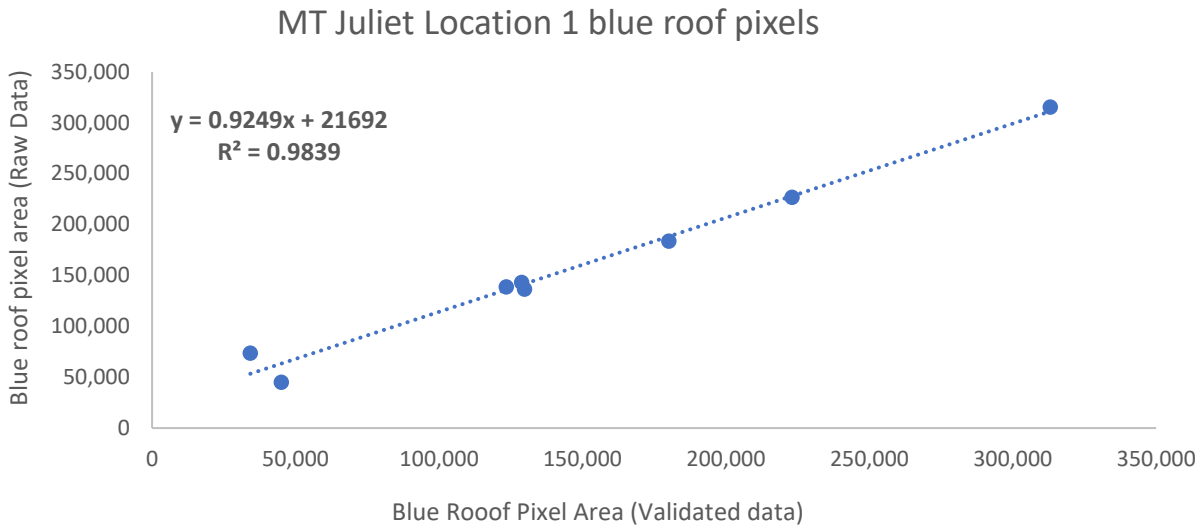

Figure 12: Linear Regression Mt Juliet Location 1

The linear regression analysis for Mt. Juliet's first location is represented in Figure *12*. The R-squared value is 0.983, indicating that approximately 98.3% of the variability observed in the raw data is also observed in the fixed data. It is important to note, the calculation of percent error for this location reached as high as 50% at the final collation period but the r-squared value of 0.983 mitigates overall trend accuracy concerns.

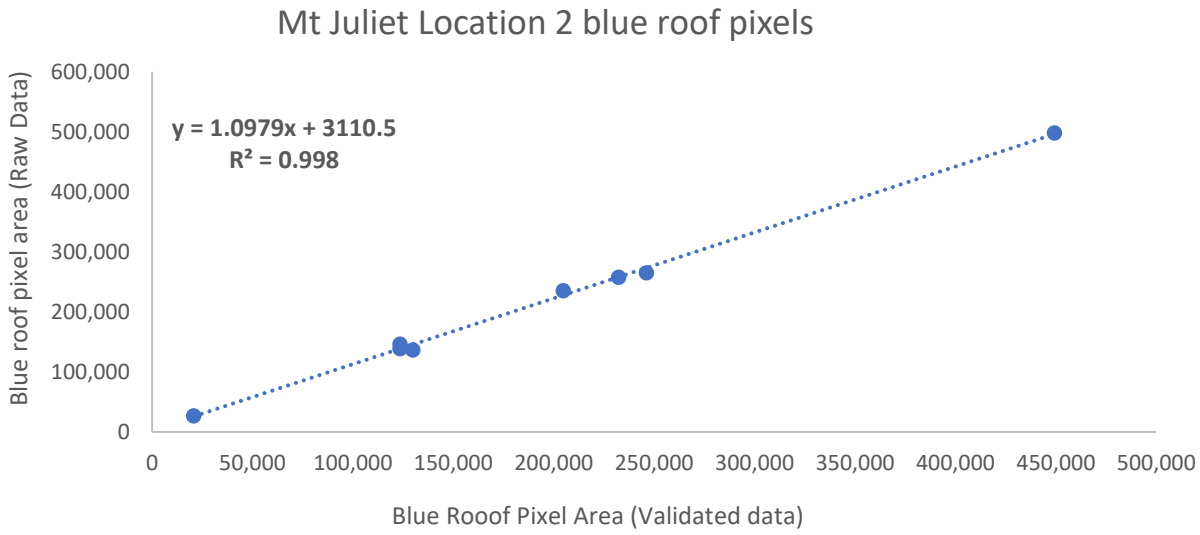

Figure 13: Linear Regression Mt Juliet Location 2

The linear regression analysis for Mt. Juliet's second location is represented in Figure 13. The R-squared value is 0.998, indicating that approximately 99.8% of the variability observed in the raw data is also observed in the fixed data. An r-squared coefficient of 99.8% indicates a robust relationship between the variables, emphasizing the reliability of the data processing techniques employed in capturing the variations in blue roof pixels.

CHAPTER 5: DISCUSSION

In the upcoming section, the attention will be on interpreting the results obtained from the methodology presented earlier. The primary object is to discuss the causes causing the important percentage errors. Highlighting East Nashville Location 1, with detailed consideration of the results from September 4th, 2020. The analysis then will move on to Mt. Juliet Location 1, specifically on March 29th, 2020. Lastly, Mt. Juliet Location 2 on to June 12th, 2020, bring together on the analysis of false positives and their impacts on the results derived from the different methodologies.

September 29 East Nashville Location 1

To enable the discussion, Figure *14* represent the location before and after the correction process, highlighting the detection and rectification of false positives. As is indicated in Table *2*, this specific date exhibits a percentage error of 24.98%, marking it as the most crucial date within the evaluation period for this specific location.

Figure 14: East Nashville, location 1, 4th September.

The initial image highlights areas where the software faced challenges in identifying the blue roofs, particularly around features like pools, blue facades of houses and fences dividing the property areas. In this set of images, the specific number of pixels identified as part of a blue roof before and after the correction process is shown in Table 4.

The R^2 value for the location over the several collection period is 99.9%, signifying the model is valuable at identifying the blue roofs. The misidentification of the fences is irrelevant for the R^2

value, but the percent error does reach 24.98% on this last date of collection. This high percent error can be explained by the fewer blue roofs areas as the recovery phase is near completion, amplifying the impression of false positives.

March 29 Mt Juliet Location 1

Mt. Juliet Location 1 presents various challenges for the software's identification of blue roofs, as evident in Figure 15. The percentage error for this specific date and location is 5.12%, making it the location with the highest percentage error values; however, the R2 value for the evaluation period remains high at 0.983 as is shown in Table 2. This high error rate can be attributed to the presence of different colors of debris in the area due to the ongoing recovery process. The diverse range of debris colors poses a significant challenge for the software's accurate identification of blue roof sheeting in this location.

Figure 15: Mt Juliet, Location 1, March 29, 2020.

The software struggled in discriminate between blue roofs and other blue-toned elements during the recovery processes, directing to a increase in false positives in its estimations. One notable example is the consistent misclassification of pool covers on certain houses as blue roofs across multiple dates. Another commonly misinterpreted is the blue doors of containers situated beside the first house on the left side of the street. Although not being actual roofing materials, these blue doors consistently are considered as false positives in the software's analysis. Overall, the

software represents a powerful tool for assessing and monitoring the recovery process, offering a convenient and competent means of evaluating post-disaster rehabilitation efforts.

June 12 Mt Juliet Location 2

This location experiences different processes during the recovery phase. Some houses were demolished, while others were nearly finished by the end of the 7-month evaluation period. With fewer houses in this area, the methodology offers a clearer insight into how effectively it analyzes recovery trends after a natural disaster.

Figure 16: Mt Juliet, Location 2, 12th June 2020.

The percentage error for the Location 2 in Mt. Juliet is detailed in Table *2*. On June 12th, Mt. Juliet (location 2) has a percent error of 18.27%. It's evident that the recovery process for the houses undergoing repairs is nearing completion. Consequently, contributing to the observed low pixel area values. Despite the substantial error percentage, it is predominantly from false positives. The software erroneously identifies a small section of the blue facade of the second house and interprets the fence as a blue roof.

Furthermore, it's important to note that the R-squared value for this location stands at 99.8%. This high R-squared value indicates a strong correlation between the observed and predicted values, showcasing the effectiveness of the software's analysis. Although encountering with false positives, the software demonstrates precise detection of blue roof areas.

The analysis suggests valuable insights into the implementation and limits of the blue roof detection algorithm across different locations and time frames. Through the evaluation of percentage errors and linear regression analyses is distinguished the patterns in the recovery process and the algorithm's performance. While some areas exhibited strong correlations between fixed and raw data, others revealed challenges such as false positives, principally in later stages of the recovery process. These findings underscore the value of refining algorithms to reduce errors, especially as recovery efforts progress. Moreover, the discussion focuses the magnitude of employing multiple methodologies to comprehensively assess data accuracy and algorithm operation in disaster recovery contexts.

In reviewing the data from the appendices section, the significance of pixels analyzed focuses the computational complexity involved in accurately identifying and measuring blue roof areas.

Although this computational challenge, the software demonstrates notable competence in estimating blue roof coverage across varied locations and timeframes. Considering that the images are captured in 4K resolution, which poses high levels of detail, the scale of pixels analyzed features the computational complexity involved in accurately identifying and measuring blue roof areas.

CHAPTER 6: CONCLUSIONS

In the wake of natural disasters, evaluating the extent of damage and tracking recovery progress is crucial for effective resource allocation and decision-making. The introduction of automated image analysis techniques offers a promising avenue for assessing post-disaster rehabilitation efforts in a cost-effective and efficient manner. This study aimed to leverage such techniques to track "blue roofs" as a metric for disaster recovery evaluation following the 2020 Tornados in Tennessee. By employing low-cost drone technology (i.e., modern consumer-level drones), this case study seeks to provide a novel and cost-effective approach to utilizing drone imagery and visual recovery cues to evaluate disaster recovery.

This study tries to provide a proof-of-concept for a methodology to evaluate disaster response processes and recovery progress over a period of time. Conventional methods of post-disaster evaluation efforts often require massive manual labor and time-intensive field surveys, making them impractical for rapidly evolving disaster scenarios. By harnessing the power of automated image analysis and modern drone imagery, this study overcomes limitations to provide timely awareness into recovery dynamics. By low-cost drone technology and active automated image analysis techniques, these results suggest the tracking of “blue roofs" serve as an precise metric for disaster recovery evaluation.

An analysis conducted in this study has founded several findings that underscore the effectiveness and possible tests associated with automated disaster recovery assessment, Firstly, the trends observed in the "blue roof" pixel area analysis, as depicted in Figure *4* and Figure *5*,

reveal a declining trend in the number of "blue roofs" over a seven-month period following the disaster. This reduction in "blue roofs" assists as a promising guide of progress towards recovery and focusses the utility of automated image analysis in tracking recovery dynamics.

However, the certification of the automated model revealed certain limitations and challenges. The manifestation of false positive "blue roof" identifications, specifically in later stages of the recovery process, resulted in bigger percentage error, as illustrated in Table 2. These false positives, recognized to components such as adjustments in recovery processes and lighting conditions. Although these encounters with individual percentage errors, the study emphasizes the potential of automated image analysis techniques in disaster recovery assessment by identifying the acceptable R^2 values for each location.

This study offers valuable insights into recovery trends and dynamics, that can inform decision-making processes and resource allocation efforts in post-disaster scenarios. In conclusion, the study represents a significant step forward in the field of disaster recovery evaluation with further research and refinement necessary to address the identified limitations and challenges.

Future iterations of the automated model should focus on investigating internal classification errors and improving accuracy by reducing false positives. An investigation into and the delineation of systematic error in the model is a valuable next contribution that could support future implementations.

In addition, the results from this study require cross-comparison with various socio-economic metrics to further analyze the data for potential causation and correlations. The integration of

social vulnerability variables into evaluating the methodology; more specifically, one implementation method can select case-study locations based on social vulnerability and provide results with pre-defined community disposition and expectations for recovery dynamics.

Additional possible extensions can also include the integration of advanced machine learning algorithms, such as convolutional neural networks (CNN). These technologies have shown promise in enhancing the accuracy of the image recognition tasks. By implementing the power of machine learning, research can improve the operation of the automated model and classify not only the blue roofs but also more damaged features, such as debris and mobilization roads after the natural catastrophe [65].

REFERENCES

[1] J. McAneney, D. McAneney, R. Musulin, G. Walker, and R. Crompton, "Government-sponsored natural disaster insurance pools: A view from down-under," *International Journal of Disaster Risk Reduction*, vol. 15. Elsevier Ltd, pp. 1–9, Mar. 01, 2016. doi: 10.1016/j.ijdrr.2015.11.004.

[2] F. Ghesquiere and O. Mahul, "Financial Protection of the State against Natural Disasters A Primer," 2010. [Online]. Available: http://econ.worldbank.org.

[3] L. Tascón-González, M. Ferrer-Julià, M. Ruiz, and E. García-Meléndez, "Social vulnerability assessment for flood risk analysis," *Water (Switzerland)*, vol. 12, no. 2, Feb. 2020, doi: 10.3390/w12020558.

[4] P. Fernandez, S. Mourato, and M. Moreira, "Social vulnerability assessment of flood risk using GIS-based multicriteria decision analysis. A case study of Vila Nova de Gaia," *Geomatics, Natural Hazards and Risk*, vol. 7, no. 4, pp. 1367–1389, Jul. 2016, doi: 10.1080/19475705.2015.1052021.

[5] M. Alizadeh *et al.*, "Social vulnerability assessment using artificial neural network (ANN) model for earthquake hazard in Tabriz city, Iran," *Sustainability (Switzerland)*, vol. 10, no. 10, Sep. 2018, doi: 10.3390/su10103376.

[6] K. Rand and C. H. Fleming, "An interdisciplinary review to develop guidelines for modeling population displacement as a function of infrastructure reconstruction decisions," *Transp Res Interdiscip Perspect*, vol. 3, Dec. 2019, doi: 10.1016/j.trip.2019.100072.

[7] V. A. Mugabe, E. S. Gudo, O. F. Inlamea, U. Kitron, and G. S. Ribeiro, "Natural disasters, population displacement and health emergencies: Multiple public health threats in Mozambique," *BMJ Glob Health*, vol. 6, no. 9, Sep. 2021, doi: 10.1136/bmjgh-2021-006778.

[8] Y. Guo *et al.*, "A Drone-Based Sensing System to Support Satellite Image Analysis for Rice Farm Mapping," *International Geoscience and Remote Sensing Symposium (IGARSS)*, pp. 9376–9379, Jul. 2019, doi: 10.1109/IGARSS.2019.8898638.

[9] P. C. Gray *et al.*, "Integrating drone imagery into high resolution satellite remote sensing assessments of estuarine environments," *Remote Sens (Basel)*, vol. 10, no. 8, Aug. 2018, doi: 10.3390/rs10081257.

[10] F. Greenwood, E. L. Nelson, and P. Gregg Greenough, "Flying into the hurricane: A case study of UAV use in damage assessment during the 2017 hurricanes in Texas and Florida," *PLoS One*, vol. 15, no. 2, Feb. 2020, doi: 10.1371/journal.pone.0227808.

[11] C. Latham, P. Mccourt, and C. Larkin, "Natural Disasters in Australia: Issues of funding and insurance Gold Coast."

[12] Z. Aidi and H. Farida, "Natural disaster insurance for Indonesia disaster management," vol. 12, no. 2, 2020, Accessed: Nov. 30, 2023. [Online]. Available: http://www.aes.bioflux.com.ro

[13] A. De Janvry, A. Del Valle, and E. Sadoulet, “Insuring Growth The Impact of Disaster Funds on Economic Reconstruction in Mexico,” 2016. [Online]. Available: http://econ.worldbank.org.

[14] W. G. Peacock, S. Van Zandt, Y. Zhang, and W. Highfield, “Inequities in long-term housing recovery after disasters: Journal of the American Planning Association, 2014,” in *The Affordable Housing Reader*, Taylor and Francis, 2022, pp. 415–433. doi: 10.4324/9780429299377-36.

[15] NOAA, “U.S. 2020 Billion-Dollar Weather and Climate Disasters.” [Online]. Available: https://www.ncdc.noaa.gov/billions/

[16] K. Saito *et al.*, “Indicators for Measuring, Monitoring and Evaluating Post-Disaster Recovery Production and consumption of the built environment View project Energy View project 6th International Workshop on Remote Sensing for Disaster Applications Indicators for Measuring, Monitoring and Evaluating Post-Disaster Recovery,” 2008. [Online]. Available: https://www.researchgate.net/publication/333676538

[17] F. Yamazaki, T. T. Vu, and M. Matsuoka, “Context-based detection of post-disaster damaged buildings in urban areas from satellite images.”

[18] J. Horney, C. Dwyer, M. Aminto, P. Berke, and G. Smith, “Developing indicators to measure post-disaster community recovery in the United States,” *Disasters*, vol. 41, no. 1, pp. 124–149, Jan. 2017, doi: 10.1111/disa.12190.

[19] M. Aljehani and M. Inoue, “Performance evaluation of multi-UAV system in post-disaster application: Validated by HITL simulator,” *IEEE Access*, vol. 7, pp. 64386–64400, 2019, doi: 10.1109/ACCESS.2019.2917070.

[20] H. S. Munawar, A. W. A. Hammad, S. T. Waller, M. J. Thaheem, and A. Shrestha, “An integrated approach for post-disaster flood management via the use of cutting-edge technologies and UAVs: A review,” *Sustainability (Switzerland)*, vol. 13, no. 14. MDPI AG, 2021. doi: 10.3390/su13147925.

[21] W. Zhang, X. Xu, and X. Chen, “Social vulnerability assessment of earthquake disaster based on the catastrophe progression method: A Sichuan Province case study,” *International Journal of Disaster Risk Reduction*, vol. 24, pp. 361–372, Sep. 2017, doi: 10.1016/j.ijdrr.2017.06.022.

[22] M. Phillips, D. Smith, H. Brooking, and M. Duer, “Re-placing displacement in gentrification studies: Temporality and multi-dimensionality in rural gentrification displacement,” *Geoforum*, vol. 118, pp. 66–82, Jan. 2021, doi: 10.1016/j.geoforum.2020.12.003.

[23] R. Atkinson, “The hidden costs of gentrification: Displacement in central London,” 2000.

[24] B. Preis, A. Janakiraman, A. Bob, and J. Steil, “Mapping gentrification and displacement pressure: An exploration of four distinct methodologies,” *Urban Studies*, vol. 58, no. 2, pp. 405–424, Feb. 2021, doi: 10.1177/0042098020903011.

[25] N. Nikhil, S. M. Shreyas, G. Vyshnavi, and S. Yadav, “Unmanned aerial vehicles (UAV) in disaster management applications,” *Proceedings of the 3rd International Conference on Smart Systems and Inventive Technology, ICSSIT 2020*, pp. 140–148, Aug. 2020, doi: 10.1109/ICSSIT48917.2020.9214241.

[26] S. Lee and Y. Choi, “Reviews of unmanned aerial vehicle (drone) technology trends and its applications in the mining industry,” *Geosystem Engineering*, vol. 19, no. 4, pp. 197–204, Jul. 2016, doi: 10.1080/12269328.2016.1162115.

[27] K. B. Sandvik and K. Lohne, “The Rise of the Humanitarian Drone: Giving Content to an Emerging Concept,” *Millennium: Journal of International Studies*, vol. 43, no. 1, pp. 145–164, Sep. 2014, doi: 10.1177/0305829814529470.

[28] C. A. F. Ezequiel *et al.*, “UAV aerial imaging applications for post-disaster assessment, environmental management and infrastructure development,” *2014 International Conference on Unmanned Aircraft Systems, ICUAS 2014 - Conference Proceedings*, pp. 274–283, 2014, doi: 10.1109/ICUAS.2014.6842266.

[29] H. Gupta and O. P. Verma, “Monitoring and surveillance of urban road traffic using low altitude drone images: a deep learning approach,” *Multimed Tools Appl*, vol. 81, no. 14, pp. 19683–19703, Jun. 2022, doi: 10.1007/s11042-021-11146-x.

[30] F. Jalled and I. Voronkov, “Object Detection using Image Processing,” Nov. 2016, Accessed: Nov. 30, 2023. [Online]. Available: https://arxiv.org/abs/1611.07791v1

[31] A. M. V and D. M. Khan, “Recent Trends on Object Detection and Image Classification: A Review.”

[32] “(2) LinkedIn.” Accessed: Mar. 20, 2024. [Online]. Available: https://www.linkedin.com/pulse/how-much-drone-cost-different-types-drones-usman-khan-5ovff/

[33] “Buy DJI Mini 2 SE - DJI Store.” Accessed: Apr. 09, 2024. [Online]. Available: https://store.dji.com/product/dji-mini-2-se?vid=132621

[34] “Buy Matrice 350 RTK Worry-Free Basic Combo - DJI Store.” Accessed: Apr. 09, 2024. [Online]. Available: https://store.dji.com/product/m350-rtk-and-dji-care-enterprise-basic?vid=141411

[35] S. Gowroju and N. Santhosh Ramchander, “Applications of drones-a review,” *Drone Technology: Future Trends and Practical Applications*, pp. 183–206, May 2023, doi: 10.1002/9781394168002.CH8.

[36] L. Apvrille, T. Tanzi, and J. L. Dugelay, “Autonomous drones for assisting rescue services within the context of natural disasters,” *2014 31th URSI General Assembly and Scientific Symposium, URSI GASS 2014*, Oct. 2014, doi: 10.1109/URSIGASS.2014.6929384.

[37] L. K. Prakash, S. Kumar Ravva, M. Rathnamma, and G. Suryanarayana, “AI Applications of Drones,” pp. 153–182, 2023, doi: 10.1002/9781394168002.ch7.

[38] “DJI - Official Website.” Accessed: Apr. 07, 2024. [Online]. Available: https://www.dji.com/mini-2-se/specs

[39] Z. Tang, X. Liu, H. Chen, J. Hupy, and B. Yang, “Deep Learning Based Wildfire Event Object Detection from 4K Aerial Images Acquired by UAS,” *AI 2020, Vol. 1, Pages 166-179*, vol. 1, no. 2, pp. 166–179, Apr. 2020, doi: 10.3390/AI1020010.

[40] U.S. Army Corps of Engineers, “Temporary Roofing Fact Sheet.” Accessed: Nov. 30, 2023. [Online]. Available: https://www.usace.army.mil/Media/Fact-Sheets/Fact-Sheets-View/Article/475463/temporary-roofing/

[41] “Image Analysis Software | Scientific Image Analysis | Processing.” Accessed: Apr. 07, 2024. [Online]. Available: https://www.mipar.us/

[42] N. N. W. S. US Department of Commerce, “Enhanced Fujita Scale”.

[43] Daniel and Perrucci, “2020 Tornado Gallery.” Accessed: Nov. 30, 2023. [Online]. Available: https://www.tntornado2020.com/gallery-details

[44] Scott Sistek, “Nashville’s scars still healing two years after deadly tornado outbreak,” tps://www.foxweather.com/weather-news/nashvilles-scars-still-healing-two-years-after-deadly-march-2020-tornado-outbreak.

[45] FOX17 WZTV NASHVILLE, “Three years later: Tennesseans remember lives lost in deadly March tornado,” https://fox17.com/news/local/three-years-later-tennesseans-remember-lives-lost-in-deadly-march-tornado.

[46] “Storm Events Database - Event Details | National Centers for Environmental Information.” Accessed: Nov. 30, 2023. [Online]. Available: https://www.ncdc.noaa.gov/stormevents/eventdetails.jsp?id=874370

[47] “CDC/ATSDR SVI Data and Documentation Download | Place and Health | ATSDR.” Accessed: Nov. 30, 2023. [Online]. Available: https://www.atsdr.cdc.gov/placeandhealth/svi/data_documentation_download.html

[48] “Spatial Hazard Events and Losses Database for the United States | Center for Emergency Management and Homeland Security.” Accessed: Nov. 30, 2023. [Online]. Available: https://cemhs.asu.edu/sheldus

[49] “Storm Events Database - Event Details | National Centers for Environmental Information.” Accessed: Nov. 30, 2023. [Online]. Available: https://www.ncdc.noaa.gov/stormevents/eventdetails.jsp?id=880428

[50] “Storm Events Database - Event Details | National Centers for Environmental Information.” Accessed: Nov. 30, 2023. [Online]. Available: https://www.ncdc.noaa.gov/stormevents/eventdetails.jsp?id=880546

[51] “Storm Events Database - Event Details | National Centers for Environmental Information.” Accessed: Nov. 30, 2023. [Online]. Available: https://www.ncdc.noaa.gov/stormevents/eventdetails.jsp?id=882955

[52] “Storm Events Database - Event Details | National Centers for Environmental Information.” Accessed: Nov. 30, 2023. [Online]. Available: https://www.ncdc.noaa.gov/stormevents/eventdetails.jsp?id=882999

[53] “Storm Events Database - Event Details | National Centers for Environmental Information.” Accessed: Nov. 30, 2023. [Online]. Available: https://www.ncdc.noaa.gov/stormevents/eventdetails.jsp?id=883007

[54] “Storm Events Database - Event Details | National Centers for Environmental Information.” Accessed: Nov. 30, 2023. [Online]. Available: https://www.ncdc.noaa.gov/stormevents/eventdetails.jsp?id=883009

[55] “Storm Events Database - Event Details | National Centers for Environmental Information.” Accessed: Nov. 30, 2023. [Online]. Available: https://www.ncdc.noaa.gov/stormevents/eventdetails.jsp?id=883016

[56] “Storm Events Database - Event Details | National Centers for Environmental Information.” Accessed: Nov. 30, 2023. [Online]. Available: https://www.ncdc.noaa.gov/stormevents/eventdetails.jsp?id=883048

[57] “Storm Events Database - Event Details | National Centers for Environmental Information.” Accessed: Nov. 30, 2023. [Online]. Available: https://www.ncdc.noaa.gov/stormevents/eventdetails.jsp?id=871306

[58] “East Nashville neighborhood in Nashville, Tennessee (TN), 37206, 37207, 37216 subdivision profile - real estate, apartments, condos, homes, community, population, jobs, income, streets.” Accessed: Nov. 30, 2023. [Online]. Available: https://www.city-data.com/neighborhood/East-Nashville-Nashville-TN.html

[59] “The Tennessee Tornadoes Of 2020 | WPLN News.” Accessed: Nov. 30, 2023. [Online]. Available: https://wpln.org/post/the-tennessee-tornadoes-of-2020-one-year-later/

[60] “Mount Juliet, Tennessee (TN 37076) profile: population, maps, real estate, averages, homes, statistics, relocation, travel, jobs, hospitals, schools, crime, moving, houses, news, sex offenders.” Accessed: Nov. 30, 2023. [Online]. Available: https://www.city-data.com/city/Mount-Juliet-Tennessee.html

[61] D. G. Mayer and D. G. Butler, “Statistical validation,” *Ecol Modell*, vol. 68, no. 1–2, pp. 21–32, Jul. 1993, doi: 10.1016/0304-3800(93)90105-2.

[62] O. O. Aalen, “A linear regression model for the analysis of life times,” *Stat Med*, vol. 8, no. 8, pp. 907–925, 1989, doi: 10.1002/SIM.4780080803.

[63] J. Benesty, S. Member, J. Chen, and Y. Huang, “On the Importance of the Pearson Correlation Coefficient in Noise Reduction,” *IEEE Trans Audio Speech Lang Process*, vol. 16, no. 4, p. 757, 2008, doi: 10.1109/TASL.2008.919072.

[64] O. E. Gouda and S. H. El-Hoshy, “Diagnostic technique for analysing the internal faults within power transformers based on sweep frequency response using adjusted r-square methodology,” *IET Science, Measurement and Technology*, vol. 14, no. 10, pp. 1057–4068, Dec. 2020, doi: 10.1049/IET-SMT.2020.0048.

[65] K. Zhao *et al.*, “Application research of image recognition technology based on CNN in image location of environmental monitoring UAV”, doi: 10.1186/s13640-018-0391-6.

APPENDIX

Table 4 Pixel Area Data Before and After Correction Process

Pixel Area Data Before and After Correction Process												
	East Nashville - Location 1			East Nashville - Location 2			Mt Juliet - Location 1			Mt Juliet - Location 2		
Dates in 2020	Raw	Corrected	Error %	Raw	Corrected	Error %	Raw	Corrected	Error %	Raw	Corrected	Error %
March-11	6.12E+05	6.03E+05	1.50	9.96E+04	8.89E+04	12.08	2.27E+05	2.23E+05	1.65	4.98E+05	4.49E+05	10.86
March-15	7.00E+05	7.00E+05	0.11	1.01E+05	9.96E+04	1.67	1.84E+05	1.80E+05	2.01	2.35E+05	2.05E+05	15.05
March-21	7.35E+05	7.35E+05	0.01	1.27E+05	1.24E+05	2.45	3.15E+05	3.13E+05	0.72	2.65E+05	2.46E+05	7.73
March-29	6.67E+05	6.57E+05	1.54	8.64E+04	8.75E+04	-1.32	1.36E+05	1.30E+05	5.12	1.36E+05	1.30E+05	5.12
April-4	5.15E+05	5.10E+05	0.84	8.33E+04	8.34E+04	-0.12	1.43E+05	1.29E+05	11.12	2.58E+05	2.32E+05	10.99
April-11	5.00E+05	5.10E+05	-1.98	6.03E+04	5.43E+04	11.04	1.39E+05	1.23E+05	12.35	1.39E+05	1.23E+05	12.35
June-12	2.04E+05	1.91E+05	6.87	4.17E+04	3.98E+04	4.89	7.36E+04	3.42E+04	53.47	1.46E+05	1.23E+05	18.27
September-4	9.55E+04	7.64E+04	24.98	2.02E+04	1.85E+04	9.59	4.50E+04	4.50E+04	0.00	2.67E+04	2.07E+04	28.98